An Acoustic Metamaterial-Based Sensor Capable of Multiband Filtering and Amplification

Huang Xinjing, Yan Yutian, Ma Jinyu, Li Jian, and Rui Xiaobo

***Abstract*—Dispersive acoustic metamaterials (AMMs) with graded refractive index is promising in acoustic sensing enhancement by providing acoustic rainbow trapping (ART) effect. However, previous solutions to this type of AMMs are based on 2D unit cells that require infinite or very large size in the third dimension; they cannot integrate with conventional acoustic sensors without deteriorating the ability of acoustic wave manipulation. In order to advance their practical applications, this paper proposes an axisymmetric, microphone embedded AMM device with gradient profile as well as gradient plate thickness and gradient gap width along the axis. Both numerical simulations and experiments are performed to examine the ART effect of the proposed AMM device and demonstrate its excellent capacity of acoustic pressure amplification and multi-band acoustic filtering. Deploying a microphone in the gap does not disturb the acoustic field, so the proposed AMM sensor experimentally achieves remarkable acoustic gains over one order of magnitude. Sound waves of different frequencies are picked up by microphones at different gaps, realizing the real-time spatially splitting of the sound spectrum. The proposed AMM provides excellent immunity to broadband noise and a little weak suppression of the single tone noise while significantly amplifying acoustic signals of a given frequency.**

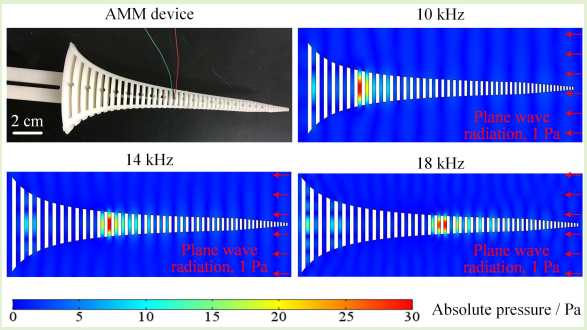

***Index Terms*—Acoustic metamaterial, rainbow trapping, acoustic sensing enhancement, artificial acoustic structure.**

I. Introduction

ACOUSTIC metamaterial (AMM), in the past two decades, has been rapidly developed. It is a kind of artificial periodic composite structure designed to manipulate sound waves with its unit cell far smaller than the acoustic wavelength [1]–[3]. AMM has many extraordinary acoustic properties such as negative equivalent density, negative equivalent bulk modulus, negative equivalent refractive index, gradient refractive index and superly large refractive index, and so on. Because of these particular properties, AMMs could yield diverse functionalities like acoustic amplification, focusing, deflection, absorption, filtering, slowing down and so on. AMMs have always been expected to advance acoustic sensing and detection technology [4], [5], [7]–[11], [13] in the form of applicable devices compatible with existing electro-acoustic conversion sensor. Therefore, activities in development of AMM devices have never stopped.

Recently, a new class of dispersive AMMs with graded refractive index (GRIN) that can slow down and trap of acoustic waves have received lots of interests, as they provide a promising prospect in acoustic sensing enhancement and precise spatial-spectral control of acoustic waves. In 2013, Zhu first experimentally demonstrated a GRIN AMM consisting of an array of grooves perforated on a rigid bar that traps broadband acoustic waves and spatially separates different frequency components, which is called acoustic rainbow trapping (ART) effect [4]. In 2014, Chen proposed an anisotropic GRIN AMM waveguide comprised of a periodic array of rectangular steel plates with linearly changed widths spaced by air gaps with equal thickness; This metamaterial realizes noticeable ART effect as well as enhanced acoustic sensing through acoustic wave compression and pressure amplification [5]. A miniature optic-fiber based acoustic point detector was used to omnidirectionally detect the complex spatial acoustic fields inside and outside this type of AMMs over a broadband

Manuscript received November 21, 2019; accepted December 23, 2019. Date of publication December 31, 2019; date of current version March 17, 2020. This work was supported by the National Natural Science Foundation of China under Grant 61803280. The associate editor coordinating the review of this article and approving it for publication was Dr. Yong Zhu. *(Corresponding author: Ma Jinyu.)*

The authors are with the State Key Laboratory of Precision Measuring Technology and Instruments, Tianjin University, Tianjin 300072, China, and also with the Binhai International Advanced Structural Integrity Research Centre, Tianjin 300072, China (e-mail: jinyu.ma@tju.edu.cn).

Digital Object Identifier 10.1109/JSEN.2019.2962279

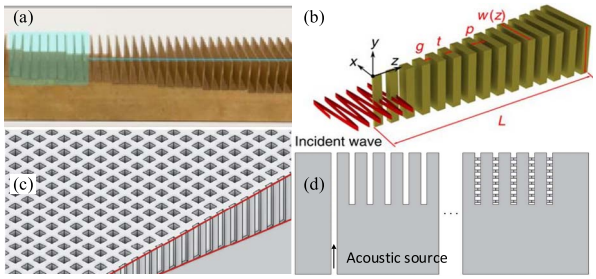

Fig. 1. Four typical AMMs with graded grooves as well as ART effect: (a) An array of grooves with graded depths on a square brass alloy bar [4]; (b) An array of stainless plates with graded widths [5]; (c) An array of square holes with graded depths on rigid material [8]; (d) An array of grooves with the same depth and width but containing several layers of crack plates with different width gaps [9].

spectrum [5], [6]. In 2014, Jia proposed a metasurface that is formed via decorating an array of grooves with graded widths on a rigid surface; Its ART effect is demonstrated via numerical simulations; The intensity of acoustic field is effectively enhanced near the propagation-stop position due to the slow group velocity [7]. In 2016, Liu used square holes as unit cell to replace previous 2D groove to construct a new type of dispersive AMM and demonstrated its ART effect via numerical simulations [8]. Lu in 2018 proposed a size-reduced ART structure by inserting several layers of crack plates in an array of air grooves decorated in the iron block with equal depth; Effective refractive indices were obtained by changing the crack gap in each plate instead of changing the groove depth [9]. Therefore, such structure can realize the wave trapping in low frequency with a reduced size. Some typical AMMs with graded grooves as well as ART effect are displayed in Fig. 1.

Besides graded grooves, there are also some other structures that are tried to construct dispersive AMMs. Esfahlani in 2016 proposed an acoustic dispersive prism structure that can split the sound waves towards different and frequency-dependent directions, while the leaky-wave nature of the structure facilitates the sound wave radiation into the ambient medium [10]. Space-coiling and micro Mie resonance-based structures are also introduced to obtain higher refractive index and deeper subwavelength scale by Ni in 2014 and Zhou in 2016 [11], [12], respectively; However, for the former, as the air gaps in space-coiling structures are too narrow to deploy a microphone, only finite element simulations were carried out to demonstrate the ART effect. Zhao in 2019 proposed a cochlear-like AMM consisting of an array of Helmholtz resonators with graded heights along a cochlear-inspired spiral tube; Acoustic pressure inside each resonator was indirectly evaluated by using a laser Doppler vibrometer to measure the vibration of the reflective tape covering the aperture on the resonator bottom [13]. Ahmed in 2015 proposed an acousto-elastic AMM model considering the ability of introducing local resonance feature to mimic the operation of human cochlea [14], [15]; However, vibration exciter instead of airborne acoustic radiation was used in testing the frequency response, so the cochlea or ART effect of such AMM has not been demonstrated effective in air. Besides acoustic waves, there are also several reports on the Lamb wave trapping [16]–[19]. These dispersive AMMs may enable a series of applications ranging from artificial cochlea to high performance acoustic sensing and filtering.

However, those AMM solutions above to obtaining dispersive or ART effect are mostly based on 2D unit cells that, in ideal cases, requiring infinite or very large size in the third direction. In the other hand, their acoustic wave manipulation capabilities are almost demonstrated in an ideal situation where the sound field is completely undisturbed; Manipulated acoustic waves are inaccessible to a real acoustic sensor; Few of them are experimentally demonstrated capable of perfectly integrating with conventional acoustic sensors without deteriorating their acoustic wave manipulation ability. This unavoidable limitation significantly restricts their further introduction to practical applications.

Therefore, this paper proposes an axisymmetric, microphone embedded AMM device with gradient profile as well as gradient plate thickness and gradient gap width along the axis that is also the wave propagation direction. Both numerical simulations and experiments are performed to examine the ART effect of the proposed AMM device and demonstrate its excellent capacity of acoustic pressure amplification, multi-band acoustic filtering, and immunity to single tone and broadband noises.

II. AMM-Based Sound Sensor Design

A. Structural Design

For those AMMs constituted by tapered plate or hole array with gradient groove depth, their equivalent density and modulus are anisotropic, and their acoustic refractive index gradually varies and are much larger than that of air, which can shorten the acoustic wavelength and concentrate the energy of sound waves in a small area. This kind of AMM can capture a certain width of planar sound waves in the vicinity of the waveguide, then longitudinally compress and amplify the sound wave inside the metamaterial, and finally concentrate the sound wave of a specific frequency at a position in the metamaterial, which is represented by the ART effect.

We make several improvements to this type of AMMs. (1) The 2D extrusion structure is changed into a 2D rotating structure so that the size of the cross section does not have to be much larger in one direction than in the other direction; the structure is slim and more compact. (2) The linear profile is changed to non-linear. In this example, the groove depth and the axial position are reciprocal to each other, so that the working frequencies of the gaps can be spatially distributed along the axial direction with equal interval. (3) In addition to the gradient profile, the thickness of each air gap and the thickness of each solid plate are also gradually reduced as the profile becomes smaller, which can reduce the heat loss caused by the air viscous effect in the narrow gaps [5], which ensures a large sound pressure gain. (4) After fully considering the distribution characteristics of the acoustic field distribution in the gap, commonly used MEMS microphones are transversely fixed in the gap, to realize sound pressure measurement in the gap without disturbing the sound field.

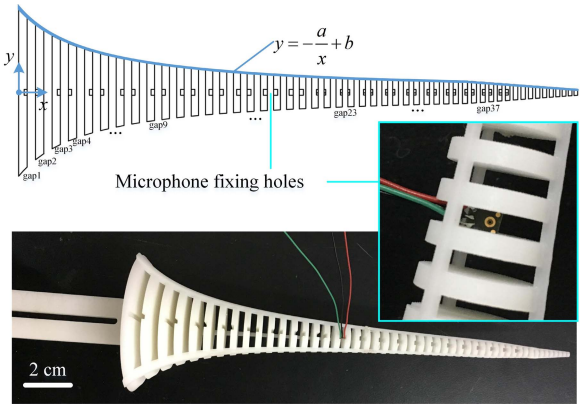

Fig. 2. Proposed axial-symmetric AMM device with microphones inserted in each gap; the device has a gradient outline and a graded refractive index (GRIN) distribution.

The newly designed AMM device is shown in Fig. 2. The scale bar is 2 centimeters. The AMM excluding the handle is 200mm long and 60mm wide at the big end. Its outline is a combined curve described by piecewise functions: $y = 738.46/x - 24.62$ for the main part and $y = -13.33x + 213.33$ for the tip part, where x and y are measured in milimeter. Such a gradual profile can have the working frequencies of each gap spatially equally spaced. The linear part is used to speed up the outline convergence so as to make the AMM not too long. The AMM consists of a series of sheets with gradient diameter, gradient thickness, and gradient gap width. The thickness t of each plate increases from 1.3 mm to 3 mm with a step of 0.035 mm as the gap radius decreases. The thickness gradient can keep the stiffness of each plate with different radius being large enough to avoid acoustic-solid coupling. The gap distance g between every two adjacent plates increases from 0.75 mm to 3 mm with a step of 0.05 mm as the gap radius decreases. The gap distance gradient can achieve a low heat loss for each gap with different radius.

It is manufactured via 3D printing, and a tiny slot is embedded at the middle of every two adjacent sheets to fix the MEMS microphone. The 3D printing material is photosensitive resin which has a Young's modulus of 2.6 GPa, and a density of 1.13 g/cm^3. What materials are used have no effect on the acoustic manipulation capabilities of the proposed device, whether plastic or metal, since the solid-gas Young's modulus contrast is 10^4-10^6 and the density contrast is 10^3-10^4. The acoustic-solid coupling can be neglectable and the solid surfaces can be treated as hard field boundaries.

B. Validation by Finite Element Simulation

Finite element simulation was carried out to demonstrate the ART effect of the designed metamaterial. Simulation configurations are shown in Fig. 3(a). 2D axisymmetric model and thermoacoustic coupled physics in frequency domain are used. The right end face are set to be plane wave radiation, while the circumferential side and left face are set as perfectly matched layers to reduce reflection interference. The rectangular area near the metamaterial is set to be a thermoacoustic domain where the mesh is refined and thermally viscous layers are added to cover the solid surface. The incident sound wave is 1 Pa, and the frequency is swept from 1 kHz to 40 kHz with a step of 500 Hz. The entire geometry is meshed into free triangles. For the entire geometry, the maximum mesh size is 1/7 wavelength. For all the gaps, the maximum mesh size is 1/2 gap width at the tip end. In the thermoacoustic domain, the number of boundary layers near the solid surface is 8 and the boundary layer stretching factor is 1.2. The simulation results referred to the acoustic pressure field are shown in Fig. 3(b)-(g). The simulation results referred to the frequency responses of each gap will be displayed later together with the experimental results. Acoustic pressure distribution only in the thermoacoustic area is displayed, not of the whole domain, in order to clearly see the bright spot in the AMM.

It can be seen from Fig. 3(b)-(g) that while the sound propagates along the axis into the metamaterial, acoustic waves of different frequencies will stop in different gaps and be amplified there. It is worth noting that in the gap where the acoustic wave stops, the sound field is uniform near the axis, and its distribution is axisymmetric due to geometric axisymmetry and is also symmetrical about any longitudinal section across the axis. If a hard boundary plane is placed across the axis, the acoustic field distribution should not change. Therefore, a MEMS microphone chip can be transversely inserted into the gap to sense the acoustic pressure amplified by the metamaterial, and the perceptual aperture of the microphone is along the y-axis. The MEMS microphone itself is an independent and complete acoustic-electrical conversion device, which only needs to supply power for. However, the needle-shaped fiber-optic microphone is cumbersome to manufacture and requires a complicated assistant system [5], [6]. It requires peripheral devices such as light source, photodetector, and FP cavity filter, and cannot accomplish acoustic pressure measurement in an embedded form. Instead, this paper can achieve perfect combination and integration of the AMM and the microphone constituting a veritable AMM-based sound sensor.

C. Theoretical Explanations

Similar to other ART metamaterials, the proposed compact 2D axisymmetric metamaterial-based sensor can gradually slow down broadband acoustic waves and have them standstill at different positions, thus trapped and spatial-spectrally separated when propagating along the metamaterial waveguide. Such ART effect is achieved by the dispersive modulation of acoustic velocity through gradually varying subwavelength unit cells that are strongly coupled along the propagation direction. The acoustic "trapped rainbow" can be released by disrupting the balance between the acoustical oscillation inside individual grooves and the mutual near-field coupling among the neighboring grooves [4].

The acoustic wave propagating along the surface of the metamaterial will lengthen its equivalent sound path due to the interaction with the sound pressure in the gaps, and the equivalent acoustic refractive index will therefore gradually become larger and larger because of sound path accumulation along the acoustic wave propagation direction. The GRIN causes longitudinal compression and amplitude magnification

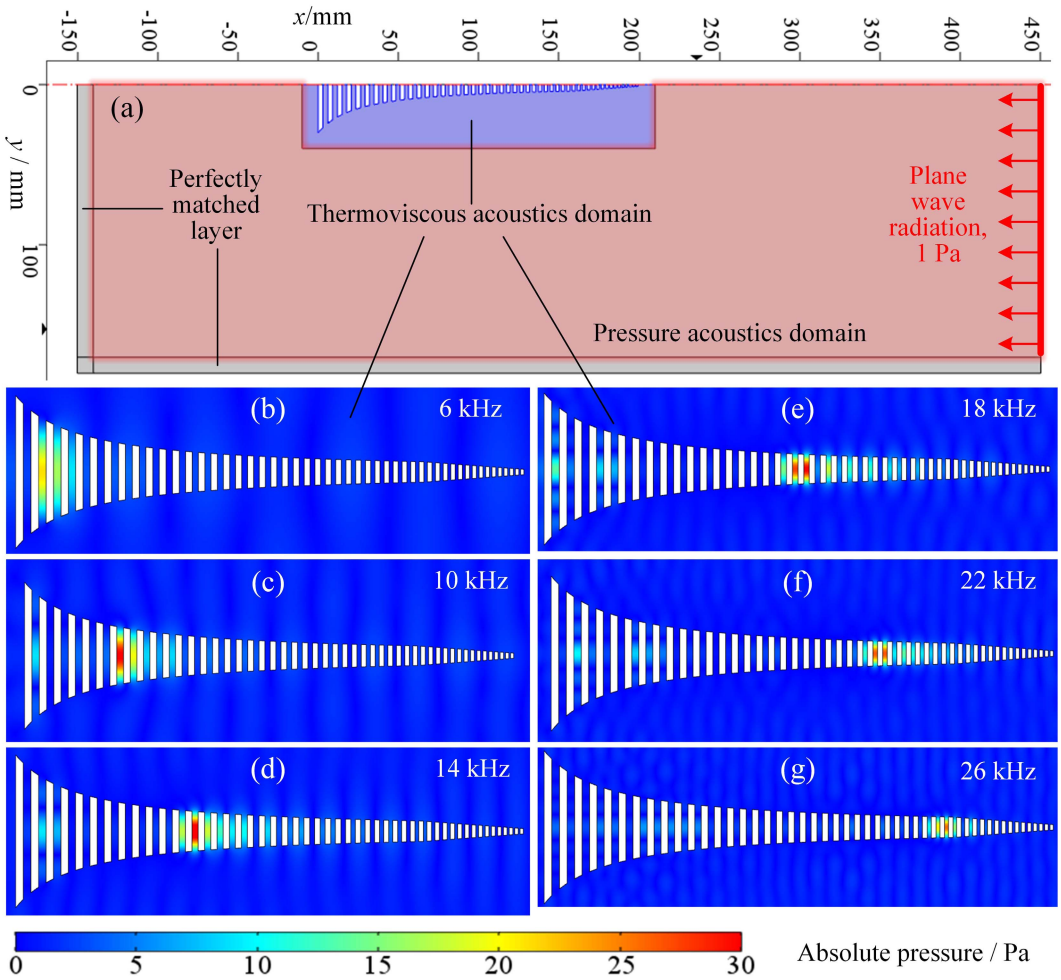

Fig. 3. ART effect of the proposed device demonstrated by FEM simulations. (a) configuration of the simulation model: A 2D axisymmetric model is adopted, and the axis is y. perfectly matched layers are attached to the left and bottom sides. The AMM is surrounded by a thermoacoustic domain in the middle of the air domain. The solid surfaces are set as hard boundary. A plane wave is incident from the right side. (b)-(g) Calculated absolute acoustic pressure inside and outside the AMM when different frequencies of acoustic waves are incident. A bright spot indicates where the sound wave stops traveling and is magnified.

of the acoustic wave [5]. In addition, gradient outline of the metamaterial waveguide can help overcome the wave vector and mode-field mismatch between the metamaterial waveguide and the background medium (air), thus enabling a high free-space (air) to metamaterial coupling efficiency.

For each groove, its working frequency that has the highest gain, is inversely proportional to the groove depth. Therefore, if the size of the metamaterial is reduced, all the working frequencies will be shifted higher. It should be noted that the ratio of the thickness to the width of the groove or plate should be matchable. If the groove is too thin, the heat loss will increase and the magnification will decrease; if the plate is too thin, the rigidity will be lowered and the plate will be easy to couple and resonate together with the air cavity, and the sound energy in the air will be thus lost.

III. Experiments

Experiment apparatus and scenario are displayed in Fig. 4. Experiments were carried out in an open field where the acoustic plane waves emitted by a loudspeaker were coupled from the free space into the metamaterial device. The transmitted signals are a series of sinusoidal waves modulated by

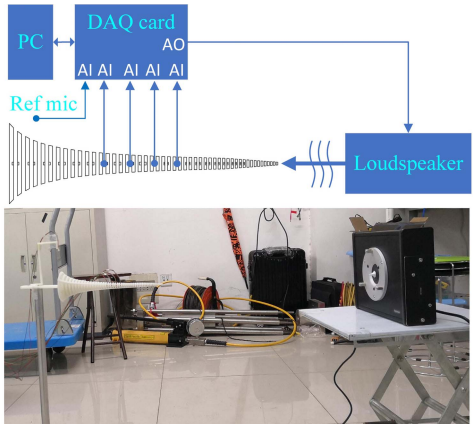

Fig. 4. Experiment apparatus. The speaker is about 1 meter away from the AMM. The acoustic wave propagates along the AMM from the tip to the big end. One microphone is placed outside the AMM to sense the incident sound pressure, and another three microphones are inserted into the AMM to sense the enhanced sound pressure. Four microphone signals are simultaneously collected by the NI capture card.

Hanning window. Output signals of the reference microphone outside the AMM and several sensing microphones inside the AMM are simultaneously acquired; The acoustic gain of the

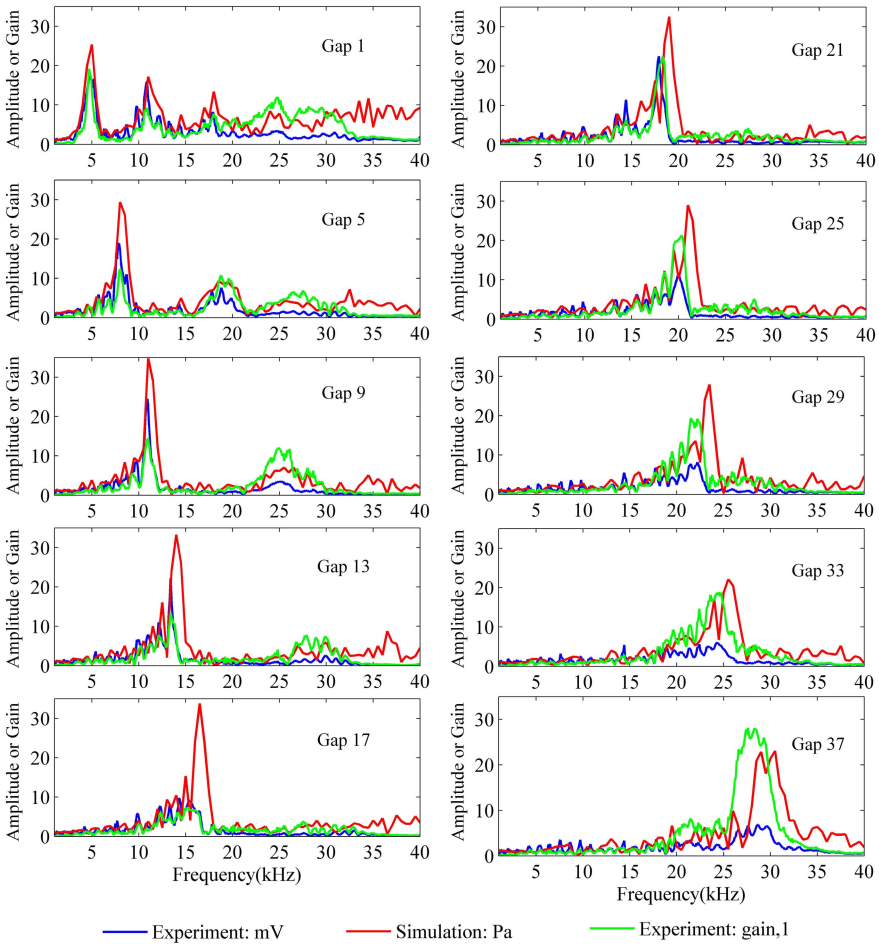

Fig. 5. Frequency responses of each gap obtained via simulations and experiments.

AMM was calculated via normalizing the latter's outputs by using the former's output. The frequency of the played sound was swept from1 kHz to 40 kHz with a step of 0.1 kHz. A total of three sets of experiments were performed: (1) Frequency sweeping experiment to test the acoustic gain and propagation-stop position of the acoustic waves of different frequencies; 19 frequency response curves of the 19 gaps in the AMM will be obtained. (2) Frequency decomposition test; A multi-frequency composite signal will be split into different gaps of the AMM. (3) Antinoise interference test, including both single tone and broadband interferences, to demonstrate the AMM can amplify a single tone at a predictable gap of the AMM and suppress broadband noises.

IV. Results and Discussions

A. Frequency Response and Acoustic Enhancement

The acoustic gain and propagation-stop position of acoustic waves of different frequencies were tested via frequency sweeping experiments. The results are shown in Fig. 5. For clear comparison, the spectra of the acoustic pressure obtained via simulations, and the microphone output and the AMM gain obtained via experiments at the positions of gaps 1, 5, 9, 13, 17, 21, 25, 29, 33, 37 are plotted together. It can be seen from the simulation results that the acoustic pressure of the incident waves is 1 Pa while the acoustic pressure at each gap is 20-30 Pa, that is to say, the theoretical acoustic gain of the proposed AMM is 20-30. Nevertheless, it can be seen from the experiment results that the actual gain is mostly 10-20 defined as the ratio of the microphone output at each gap to the reference microphone output outside the AMM. At some gaps, the acoustic magnifications are much smaller than that at other positions because the acoustic spot of adjacent gaps is split and cover two gaps. Deploying a microphone in the gap does not disturb the acoustic field a lot, so the experimental gain can maintain a high value – over one order of magnitude. The magnification for higher frequency sound is more stable and larger. As the position of the gap gradually moves toward the tip and the radius of the gap gradually becomes smaller, the characteristic frequency gradually becomes higher. The spectrum shapes of various gaps of the AMM device measured via simulations and experiments are very similar. Characteristic frequencies of higher-order mode also appear in many gaps, and the gap with a larger diameter has a denser higher-order characteristic frequency distribution.

In the experiment, a shift appears with increasing the frequency. The reason is that the printed actual AMM device is a little different from the one used in the simulation. The printed device has three support bars attached to the outer edge of those discs, while in the simulation, those discs are unsupported without bars. Those bars can slightly affect the acoustic pressure inside the gaps. The equivalent diameter of

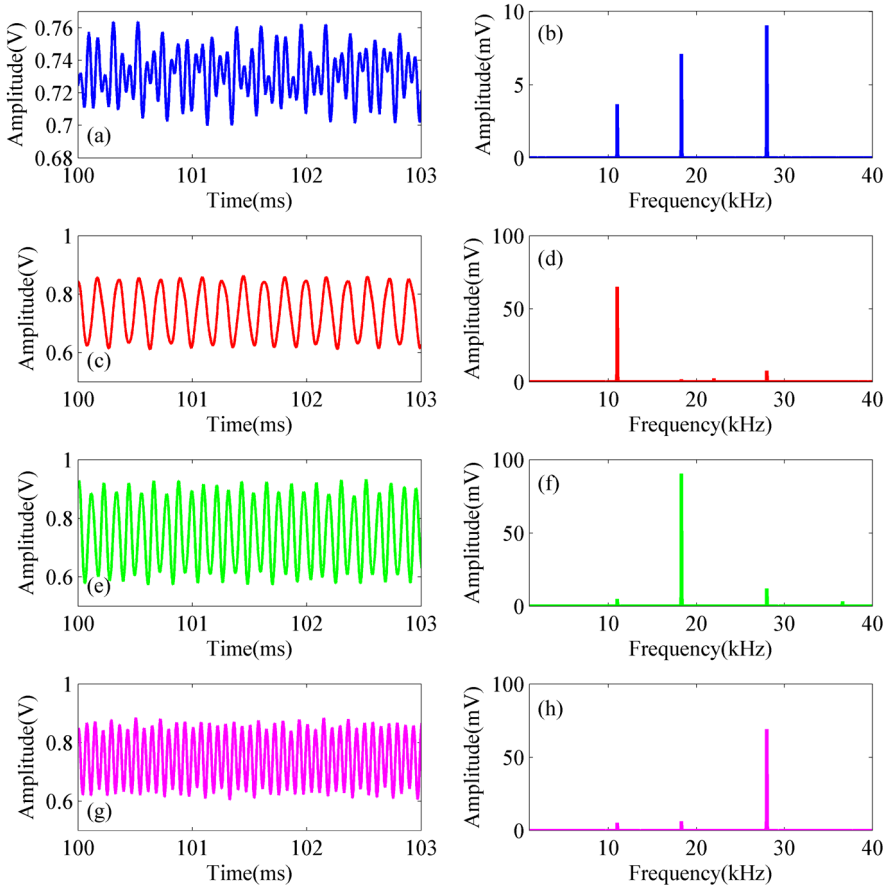

Fig. 6. Frequency decomposition functionality of the proposed device. (a): The output signal of one microphone without AMM; (b): Frequency spectrum of (a); (c), (e), (g): The output signals of three microphones that are inserted into gaps 9, 23, 37 of the AMM; (d), (f), (h): Frequency spectrums of (c), (e), (g).

each disk is slightly larger than the design value. Therefore, the resonant frequencies of each gap are a little lower than the designed values that are obtained via simulations. Gap 17 does have experimental peak, but the peak is lower than other gaps. The reason is that the bright spot of 15kHz sound are divided into two adjacent gaps. The energy split into the two gaps are not the same and the gap being tested has less energy.

B. Multi-Frequency Component Splitting

The capability of the proposed AMM device for splitting multi-frequency composite signals was tested. The sounds containing three different tones, 11kHz, 18.3 kHz, 28 kHz, were played by a loudspeaker. At first, the mixed signals were received by a single microphone without the AMM; Then, three microphones were placed in three gaps inside the AMM device characterized by these three frequencies to receive the sound. The results are shown in Fig. 6. Subgraphs in the left column are the collected signals in time domain while subgraphs in the right column are the collected signals in frequency domain calculated via fast Fourier transform. Subgraphs in the first row are the signals consisting of three frequency components: 11 kHz, 18.3 kHz, 28 kHz and collected by the single microphone without the AMM. It can be seen that the three frequency components are very noticeable. The subgraphs in the following rows are the signals collected by the three microphones at different gaps in the AMM, gaps 9, 23, and, 37, respectively, where these three frequencies overlap the three peaks of the three frequency sweeping curves. It can be seen that for each channel only the signal of its own characteristic frequency is noticeably enhanced, while the signals of other frequencies are not amplified. Sound waves of different frequencies are picked up by microphones at different gaps, realizing the spatially splitting of sound signals of different frequencies. Because such multi-frequency component splitting is real-time and uninterrupted, a simple rectification circuit can be used to realize the real-time acquisition of the amplitudes of different frequency components and realize the cochlear-like functionality.

C. Resistance to Noise Interference

Anti-interference ability of the proposed AMM device was tested. In order to generating acoustic signals containing both single tone and broadband noises, a loudspeaker is used to play two tone components of 11kHz and 18kHz, while a mobile phone was used to play a music. Music instead of noise is used because each gap of the AMM can only amplify single frequency acoustic signal, while both music and white noise are broadband in frequency domain. While noise can make people uncomfortable. The results of using music to verify the frequency-selective amplification of the AMM is the same as that of using white noise. The frequency of the music is mainly concentrated in the range of 0.1 kHz to 5 kHz. At first one microphone was used to receive such hybrid signals without the AMM; then the same microphone was

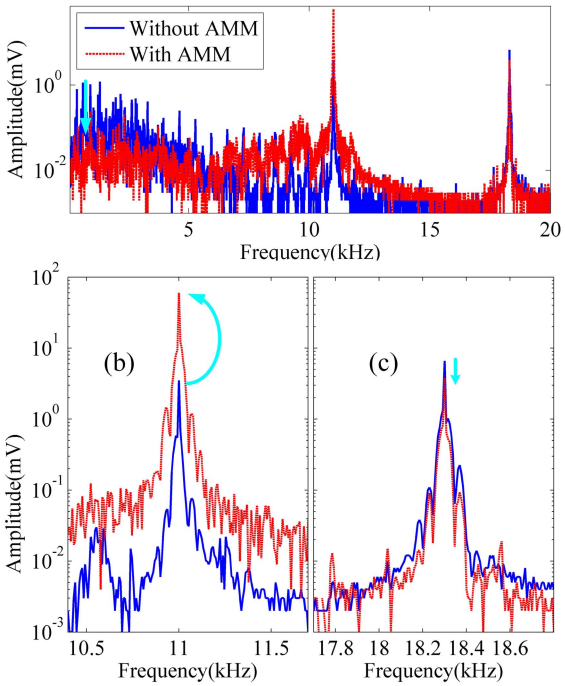

Fig. 7. Frequency selective amplification functionality of the proposed AMM device. (a) Output signals of one microphone outside the AMM and inside the gap 17 of the AMM when two tones 11 kHz and 18.3 kHz as well as a music noise are played; (b) and (c) are the details of the two peaks, enhanced and suppressed, respectively.

inserted into the gap with a characteristic frequency of 11 kHz, taking the 18 kHz sound and a piece of music played by the mobile phone as two kinds of noise interferences. The spectrums of the signals measured by the microphone in both cases are shown in Fig. 7. It can be seen that the AMM device has a strong suppression (about 10 times) for low frequency but broadband noise, a large enhancement (amplitude enhanced from 3.5 mV to 60.4 mV, 17 times) for the 11 kHz signal to be detected, and a weak suppression (amplitude attenuated from 6.6 mV to 3.8 mV, 1.7 times) for the 18 kHz interference. Therefore, the proposed AMM device has excellent anti-interference ability against broadband noise and a little weak suppression of the single tone noise while being able to significantly amplify acoustic signals of a given frequency.

V. Conclusions

This paper presents an axisymmetric, microphone embedded AMM device with a gradient profile as well as gradient plate thickness and gradient gap width along the axis. Numerical simulations were performed to examine its ART effect, while experiments were carried out to demonstrate its excellent capacity of acoustic amplification and multi-band acoustic filtering. Simulation results show that incident plane waves of different frequencies are trapped at different positions along the axis of the AMM, forming significantly enhanced sound fields. Experimental results demonstrate that deploying a microphone in the gap does not disturb the acoustic field a lot, so the experimental gain can maintain a high value – over one order of magnitude; Sound waves of different frequencies can be picked up by microphones at different gaps, realizing the real-time spatially splitting of sound signals of different frequencies; The proposed AMM device has excellent anti-interference ability against broadband noise and a little weak suppression of the single tone noise while being able to significantly amplify acoustic signals of a given frequency.

References

[1] Z. J. Wong *et al.*, "Optical and acoustic metamaterials: Superlens, negative refractive index and invisibility cloak," *J. Opt.*, vol. 19, no. 8, 2017, Art. no. 084007.
[2] S. A. Cummer, J. Christensen, and A. Alú, "Controlling sound with acoustic metamaterials," *Nature Rev. Mater.*, vol. 1, no. 3, 2016, Art. no. 16001.
[3] Y. Wu, M. Yang, and P. Sheng, "Perspective: Acoustic metamaterials in transition," *J. Appl. Phys.*, vol. 123, no. 9, 2018, Art. no. 090901.
[4] J. Zhu *et al.*, "Acoustic rainbow trapping," *Sci. Rep.*, vol. 3, p. 1728, Apr. 2013.
[5] Y. Chen, H. Liu, M. Reilly, H. Bae, and M. Yu, "Enhanced acoustic sensing through wave compression and pressure amplification in anisotropic metamaterials," *Nature Commun.*, vol. 5, p. 5247, Oct. 2014.
[6] R. Ganye, Y. Chen, H. Liu, H. Bae, Z. Wen, and M. Yu, "Characterization of wave physics in acoustic metamaterials using a fiber optic point detector," *Appl. Phys. Lett.*, vol. 108, no. 26, 2016, Art. no. 261906.
[7] H. Jia, M. Lu, X. Ni, M. Bao, and X. Li, "Spatial separation of spoof surface acoustic waves on the graded groove grating," *J. Appl. Phys.*, vol. 116, no. 12, 2014, Art. no. 124504.
[8] L. Tuo and Z. Jie, "Acoustic rainbow trapping through perforated structures," presented at the 23rd Int. Congr. Sound Vib., Ancient Mod. Acoust., Athens, Greece, Jul. 2016.
[9] L. Wenjia *et al.*, "A size-reduced acoustic rainbow trapping structure," *J. Appl. Acoust.*, vol. 37, no. 2, pp. 214–218, 2018.
[10] H. Esfahlani, S. Karkar, H. Lissek, and J. R. Mosig, "Acoustic dispersive prism," *Sci. Rep.*, vol. 6, no. 1, 2016, Art. no. 18911.
[11] X. Ni *et al.*, "Acoustic rainbow trapping by coiling up space," *Sci. Rep.*, vol. 4, Nov. 2014, Art. no. 7038.
[12] C. Zhou, B. Yuan, Y. Cheng, and X. Liu, "Precise rainbow trapping for low-frequency acoustic waves with micro Mie resonance-based structures," *Appl. Phys. Lett.*, vol. 108, no. 6, 2016, Art. no. 063501.
[13] L. Zhao and S. Zhou, "Compact acoustic rainbow trapping in a bioinspired spiral array of graded locally resonant metamaterials," *Sensors*, vol. 19, no. 4, p. 788, 2019.
[14] M. R. U. Ahmed, "Bio-inspired design of mechanical band pass sensor with the ability to scavenge energy," Ph.D. dissertation, Mech. Eng. College Eng. Comput., Univ. South Carolina, Columbia, SC, USA, 2010.
[15] F. Ma, J. H. Wu, M. Huang, G. Fu, and C. Bai, "Cochlear bionic acoustic metamaterials," *Appl. Phys. Lett.*, vol. 105, no. 21, 2014, Art. no. 213702.
[16] D. G. Zhao, Y. Li, and X. F. Zhu, "Broadband Lamb wave trapping in cellular metamaterial plates with multiple local resonances," *Sci. Rep.*, vol. 5, Mar. 2015, Art. no. 9376.
[17] E. A. Skelton, R. V. Craster, A. Colombi, and D. J. Colquitt, "The multi-physics metawedge: Graded arrays on fluid-loaded elastic plates and the mechanical analogues of rainbow trapping and mode conversion," *New J. Phys.*, vol. 20, no. 5, 2018, Art. no. 053017.
[18] Z. Tian and L. Yu, "Rainbow trapping of ultrasonic guided waves in chirped phononic crystal plates," *Sci. Rep.*, vol. 7, Jan. 2017, Art. no. 40004.
[19] T. Giuseppe, Y. Xia, J. Marconi, G. Cazzulani, A. Erturk, and M. Ruzzene, "Time-periodic stiffness modulation in elastic metamaterials for selective wave filtering: Theory and experiment," *Phys. Rev. Lett.*, vol. 122, no. 12, 2019, Art. no. 124301.